JIPB Journal of Integrative Plant Biology

Proteome analysis of peroxisomes from dark-treated senescent *Arabidopsis* leaves[FA]

Ronghui Pan[1†], Sigrun Reumann[1,2,3,4†], Piotr Lisik[3], Stefanie Tietz[1], Laura J. Olsen[2] and Jianping Hu[1,5*]

1. MSU-Department of Energy Plant Research Laboratory, Michigan State University, East Lansing, MI 48824, USA
2. Department of Molecular, Cellular, and Developmental Biology, University of Michigan, Ann Arbor, MI, USA
3. Center of Organelle Research, University of Stavanger, N-4021 Stavanger, Norway
4. Department of Plant Biochemistry and Infection Biology, Institute of Plant Science and Microbiology, University of Hamburg, D-22609 Hamburg, Germany
5. Plant Biology Department, Michigan State University, East Lansing, MI 48824, USA
†These authors contributed equally to this work
*Correspondence: Jianping Hu (huji@msu.edu)
doi: 10.1111/jipb.12670

High-Impact Article

Abstract Peroxisomes compartmentalize a dynamic suite of biochemical reactions and play a central role in plant metabolism, such as the degradation of hydrogen peroxide, metabolism of fatty acids, photorespiration, and the biosynthesis of plant hormones. Plant peroxisomes have been traditionally classified into three major subtypes, and in-depth mass spectrometry (MS)-based proteomics has been performed to explore the proteome of the two major subtypes present in green leaves and etiolated seedlings. Here, we carried out a comprehensive proteome analysis of peroxisomes from *Arabidopsis* leaves given a 48-h dark treatment. Our goal was to determine the proteome of the third major subtype of plant peroxisomes from senescent leaves, and further catalog the plant peroxisomal proteome. We identified a total of 111 peroxisomal proteins and verified the peroxisomal localization for six new proteins with potential roles in fatty acid metabolism and stress response by *in vivo* targeting analysis. Metabolic pathways compartmentalized in the three major subtypes of peroxisomes were also compared, which revealed a higher number of proteins involved in the detoxification of reactive oxygen species in peroxisomes from senescent leaves. Our study takes an important step towards mapping the full function of plant peroxisomes.

Edited by: Li-Xin Zhang, Institute of Botany, the Chinese Academy of Sciences, China
Received May 8, 2018; **Accepted** May 29, 2018; **Online on** Jun. 7, 2018
FA: Free Access, paid by JIPB

Free Access

INTRODUCTION

Peroxisomes are ubiquitous and dynamic organelles playing vital functions in eukaryotic cells. The metabolic functions of peroxisomes vary significantly among kingdoms, and even in different tissues and developmental stages of the same organism. In plants, peroxisomes have major functions in fatty acid catabolism, hydrogen peroxide (H_2O_2) degradation, photorespiration, the glyoxylate cycle, pathogen defense and the biosynthesis of important plant hormones, such as jasmonic acid (JA), indole-3-acetic acid (IAA) and salicylic acid (SA). Other peroxisomal functions include the catabolism of polyamines, uric acid, amino acids, sulfite and pseudouridine, as well as the biosynthesis of phylloquinone, isoprenoids, biotin and Coenzyme A (CoA) (Kaur et al. 2009; Hu et al. 2012; Pan and Hu 2018).

The peroxisome lacks DNA, and peroxisomal proteins are nuclear encoded and imported into the organelle by peroxins (PEX proteins), a majority of which are membrane associated. Most peroxisomal matrix proteins carry one of the two major peroxisome targeting signals (PTSs): the C-terminal tripeptide PTS1, with a canonical sequence of SKL> (> indicates the C-terminal end of the protein); and the nonapeptide PTS2, which is located in the N-terminal region and only present in a small number of matrix proteins (Sparkes and Baker 2002; Reumann et al. 2016).

To fully understand the physiological roles of plant peroxisomes, it is necessary to catalogue the proteome

of these organelles. In recent years, experimental proteomics, based on peroxisome purification and mass spectrometry (MS), have greatly accelerated the rate and scale of the identification of novel plant peroxisomal proteins (Kaur and Hu 2011; Reumann 2011; Pan and Hu 2018). This unbiased and relatively large-scale approach has not only successfully identified new auxiliary and regulatory proteins involved in established peroxisomal processes, but also revealed numerous proteins involved in unexpected peroxisomal functions (Kaur and Hu 2011; Reumann 2011; Pan and Hu 2018).

Peroxisomes are metabolically and morphologically dynamic. Environmental factors, including light, are known to cause changes in peroxisome abundance (Lopez-Huertas et al. 2000; Koh et al. 2005; Desai and Hu 2008; Rodríguez-Serrano et al. 2016; Desai et al. 2017; Fahy et al. 2017). The proteome and primary functions of plant peroxisomes vary, quantitatively and qualitatively, across developmental stages, and distinct names were given to the three major subtypes of plant peroxisomes. Leaf peroxisomes in green leaves are mainly involved in photorespiration (Tolbert et al. 1969; Peterhansel et al. 2010), glyoxysomes refer to peroxisomes in seeds/fatty tissue, which harbor the glyoxylate cycle together with fatty acid β-oxidation (Beevers 1979), and gerontosomes refer to peroxisomes in senescent tissues, which were suggested to resemble glyoxysomes in terms of their metabolic functions (Vicentini and Matile 1993).

To uncover peroxisomal proteins at different developmental stages, previous proteomic studies analyzed peroxisomes purified from various plant organs and species, including greening and etiolated *Arabidopsis* cotyledons (Fukao et al. 2002, 2003), *Arabidopsis* leaves (Reumann et al. 2007, 2009), non-green *Arabidopsis* cell suspension cultures (Eubel et al. 2008), etiolated *Arabidopsis* seedlings (Quan et al. 2013), etiolated soybean cotyledons (Arai et al. 2008), and spinach leaves (Babujee et al. 2010). These studies revealed common pathways, as well as proteins specific to certain developmental stages, and identified a number of novel peroxisome proteins, such as those involved in methylglyoxal detoxification, phylloquinone biosynthesis, pseudouridine catabolism, CoA biosynthesis, and putative regulatory proteins (Kaur and Hu 2011; Reumann 2011; Pan and Hu 2018).

The goal of this study was to discover additional peroxisomal proteins and catalog the proteome of peroxisomes from plants undergoing senescence-related processes. Senescence is a genetically-controlled global-reprogramming of cellular activities, featured by the cessation of photosynthesis, degradation of chlorophyll, disintegration of organelle structures, and degradation of diverse cellular components, such as proteins and lipids (Buchanan-Wollaston 1997). Plant peroxisomal metabolism during leaf senescence has been investigated in pea, from which increased proteolytic activity and more active metabolism of reactive oxygen species (ROS), nitric oxide and NADPH was discovered (Pastori and del Rio 1997; Corpas et al. 1999, 2004). However, analysis of the whole peroxisome proteome undergoing senescence-related processes had been lacking. Detached leaves subjected to extended (e.g. 48 h) darkness have been widely used as a system to study plant senescence (Biswal and Biswal 1984; Oh et al. 1997; Weaver et al. 1998; Weaver and Amasino 2001; Song et al. 2014; Liebsch and Keech 2016). To this end, we performed proteome analysis of peroxisomes isolated from leaves of dark-treated detached *Arabidopsis* plants. This study identified 111 peroxisomal proteins, a higher number compared with previous peroxisome proteomic studies in any organism, with eight being identified for the first time by MS-based proteomics of peroxisomes. Our *in vivo* subcellular targeting analysis validated peroxisomal localization of six new proteins involved in fatty acid metabolism and stress response. Our study takes an important step towards fully deciphering the peroxisome proteome and uncovering novel physiological roles of plant peroxisomes.

RESULTS

Mass spectrometry-based interrogation of peroxisomal proteins

Isolation of leaf peroxisomes requires large amounts of leaves (approximately 60 g FW). Therefore, any abiotic stress applied to *Arabidopsis* plants needs to reach all leaves and preferentially all mesophyll cells relatively uniformly. A comparison of intact and harvested *Arabidopsis* Col-0 plants subjected to prolonged dark treatment demonstrated that only harvested plants showed uniform progression of leaf senescence in all leaves, consistent with previous reports of chlorophyll degradation (see Introduction). The chlorophyll content

was reduced by approximately 40% after 48 h of dark-induced senescence, and reached a residual level of approximately 15% after 4 d (Figure 1A). By contrast, when intact plants were subjected to dark treatment, leaf senescence became visible only slowly and primarily in the oldest leaves, and as a result, chlorophyll content of the entire plant hardly declined, even after 6 d (Figure S1A). As such, we chose harvested plants for dark treatment to induce uniform leaf senescence.

After 4 weeks of growth under a 16/8 h light/dark cycle, the above-ground portion of *Arabidopsis* plants was harvested and subjected to 48 h dark treatment (Figure S1B), at which point peroxisomes were isolated and purity assessed (Figure 1B), using our previously established immunological methodologies (Reumann et al. 2009; Quan et al. 2013). Two independent pools of peroxisome preparations with maximum purity, named Total 1 (T1) and Total 2 (T2), were obtained. For protein identification, 500 μg each of T1 and T2 peroxisome proteins were separated on a 1D gel, which was later sliced into eight pieces after electrophoresis. Proteins in each slice were *in-gel* digested by trypsin, and subjected to liquid chromatography-electrospray ionization-tandem mass spectrometry (LC-ESI-MS/MS). This method had been used in our previous studies to successfully identify a large number of peroxisomal proteins from peroxisomes of *Arabidopsis* etiolated seedlings and green leaves (Reumann et al. 2007, 2009; Quan et al. 2013).

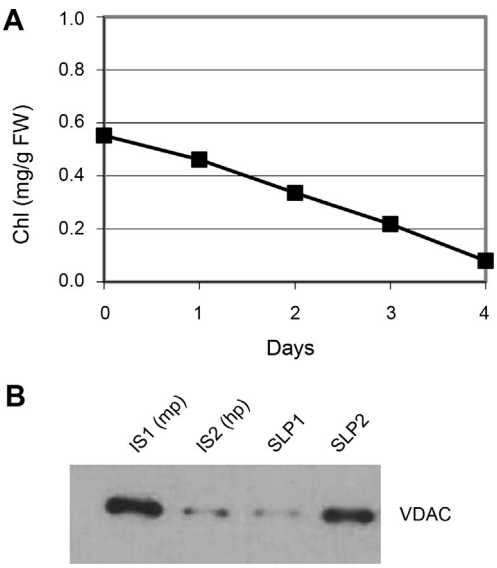

Figure 1. Assessment of dark-induced senescence in *Arabidopsis* and purity of isolated leaf peroxisomes
(A) Change in chlorophyll content (mg chl/g FW) during dark-induced senescence of detached *Arabidopsis* shoots. **(B)** Immunoblot of different leaf peroxisome isolates (5 μg protein/each preparation) from senescent shoots using an anti-VDAC (voltage-dependent anion channel) antibody (Reumann et al. 2009) to determine the degree of mitochondrial contamination. Two internal standards (IS1-2) of moderate (mp) and high purity (hp) were analyzed, in parallel, to compare the degree of contamination between different isolates. Senescent leaf peroxisome isolates of highest purity (e.g., SLP1) were selected and pooled with other high-purity isolates for proteome analysis by mass spectrometry.

Using 99% probability of protein identification as the cut-off, a total of 320 and 391 proteins were detected in T1 and T2, respectively (Table S1). Among them, 91 proteins from T1 and 100 proteins from T2 (105 proteins in total) were previously established peroxisomal proteins (Table 1). To identify putative novel peroxisome proteins, the remaining proteins were further classified into 'non-peroxisomal' and 'potentially new peroxisomal', using protein subcellular localization information in the *Arabidopsis* Subcellular Proteomic Database (SUBA4) (Hooper et al. 2017), which represents compiled data from published biochemical studies, organelle proteomics, and/or fluorescence microscopy-based localization analyses. Also included in the 'potentially new peroxisomal' category were five proteins annotated as non-peroxisomal by SUBA, but contained C-terminal PTS1 or PTS1-like tripeptides. These included fructose-bisphosphate aldolase 1 splicing isoform 2 (FBA1.2; SFL>), glutamate-1-semialdehyde 2,1-aminomutase 1 (GSA1; SRI>), aconitate hydratase 3 (ACO3; SKQ>), TSK-associating protein 1 (TSA1; SSL>), and 60S ribosomal protein L19-1 (RPL19A; SKK>). In total, 211 proteins from T1 and 267 proteins from T2 were considered as 'non-peroxisomal' (Table S2), and together 30 proteins were considered to be 'potentially new peroxisomal' proteins (Table S3).

Microscopic validation of peroxisomal localization

Due to possible organelle contamination, all novel proteins detected by mass spectrometry- based organelle proteomics need to be confirmed by an independent approach, such as *in vivo* subcellular targeting analysis of fluorescently tagged candidate proteins. To uncover new peroxisomal proteins and functions, we selected 19 out of the 30 potentially new peroxisomal proteins (Table S3) for *in vivo* targeting analysis. The following selection criteria were applied: (i) the presence of a PTS-like sequence; (ii) having putative

Table 1. Peroxisomal proteins identified in this study

Pathway/annotation	Symbol	At locus	PTS1/2	Protein identification T1	Protein identification T2
β-oxidation					
3-Ketoacyl-CoA thiolase 1	KAT1	AT1G04710	RQx_5HL	X	X
Acyl-CoA oxidase 3	ACX3	AT1G06290	RAx_5HI/SSV	X	X
Acyl-activating enzyme 1	AAE1	AT1G20560	SKL	X	X
3-Ketoacyl-CoA thiolase 2	KAT2	AT2G33150	RQx_5HL	X	X
Acyl-CoA oxidase	ACX5	AT2G35690	AKL	X	X
Long-chain acyl-CoA synthetase 6	LACS6	AT3G05970	RIx_5HL	X	X
Multifunctional protein 2	MFP2	AT3G06860	SRL	X	X
Hydroxybutyryl-CoA dehydrogenase	HBCDH	AT3G15290	PRL	X	X
Acyl-activating enzyme 7	AAE7	AT3G16910	SRL	X	X
Acyl-CoA oxidase 4	ACX4	AT3G51840	SRL	X	X
Acyl-CoA oxidase 1	ACX1	AT4G16760	ARL	X	X
Abnormal inflorescence meristem 1	AIM1	AT4G29010	SKL	X	X
Acyl-activating enzyme 5	AAE5	AT5G16370	SRM	X	X
Acyl-activating enzyme 17	AAE17	AT5G23050	SKL	X	X
Long-chain acyl-CoA synthetase 7	LACS7	AT5G27600	RLx_5HI/SKL	X	X
3-Ketoacyl-CoA thiolase 5	KAT5	AT5G48880	RQx_5HL	X	X
Acyl-CoA oxidase 2	ACX2	AT5G65110	RIx_5HL	X	
IAA biosynthesis (β-oxidation)					
Indole-3-butyric acid response 3	IBR3	AT3G06810	SKL	X	X
Short-chain dehydrogenase-reductase a/Indole-3-butyric acid response 1	IBR1	AT4G05530	SRL	X	X
JA biosynthesis (β-oxidation)					
OPC-8:0 ligase 1	OPCL1	AT1G20510	SKL	X	X
12-oxophytodienoate reductase 3	OPR3	AT2G06050	SRL	X	X
4-coumarate:CoA ligase 1	4CL1	AT4G05160	SKM	X	X
4-coumarate:CoA ligase like 2	4CL2	AT5G63380	SKL	X	X
Auxiliary β-oxidation and other fatty acid catabolism					
Small thioesterase 4	st4	AT1G04290	SNL		X
Δ^3,Δ^2-enoyl CoA isomerase 1	ECI1	AT1G65520	SKL	X	
Monofunctional enoyl-CoA hydratase 2	ECH2	AT1G76150	SSL	X	X
Peroxisomal NAD^+-malate deshydrogenase 1	PMDH1	AT2G22780	RIx_5HL	X	X
Small thioesterase 5	st5	AT2G29590	SKL	X	X
Short-chain dehydrogenase-reductase c	SDRc	AT3G01980	SYM	X	X
Short-chain dehydrogenase-reductase b/ 2,4-dienoyl-CoA reductase	SDRb/ DECR	AT3G12800	SKL	X	X
Hydroxy-acid oxidase 1	HAOX1 # $	AT3G14130	SML		X
Hydroxy-acid oxidase 2	HAOX2	AT3G14150	SML		X
Short-chain dehydrogenase-reductase d	SDRd	AT3G55290	SSL	X	X
Short-chain dehydrogenase-reductase e	SDRe # $	AT3G55310	SSL	X	

(Continued)

Table 1. Continued

Pathway/annotation	Symbol	At locus	PTS1/2	Protein identification T1	Protein identification T2
Small thioesterase 3	st3	AT3G61200	SKL	X	X
Epoxide hydrolase 3	EH3	AT4G02340	ASL	X	X
Indole-3-butyric acid response 10/ $\Delta^{(3)}$, $\Delta^{(2)}$-Enoyl-CoA isomerase 2	IBR10/ ECI2	AT4G14430	PKL	X	X
Monofunctional enoyl-CoA hydratase/isomerase a	ECHIa	AT4G16210	SKL	X	X
Peroxisomal NAD+-malate deshydrogenase 2	PMDH2	AT5G09660	RIx_5HL	X	X
Sterol carrier protein 2	SCP2	AT5G42890	SKL	X	X
$\Delta 3^{,5}$-$\Delta^{2,4}$-dienoyl-CoA-isomerase	DCI1	AT5G43280	AKL	X	X
Photorespiration					
Glutamate-glyoxylate aminotransferase 1	GGT1	AT1G23310	SKM	X	X
Hydroxypyruvate reductase 1	HPR1	AT1G68010	SKL	X	X
Glutamate-glyoxylate aminotransferase 2	GGT2	AT1G70580	SRM	X	X
Serine-glyoxylate aminotransferase/ Alanine:glyoxylate aminotransferase 1	SGT/ AGT1	AT2G13360	SRI	X	X
Glycolate oxidase 1	GOX1	AT3G14415	PRL	X	X
Acyl-CoA hydrolysis					
Acyl-CoA thioesterase 2	ACH2	AT1G01710	SKL	X	X
AcylCoA thioesterase family protein	ACH	AT4G00520	AKL		X
Biogenesis					
Peroxin 11c	PEX11c	AT1G01820		X	X
Peroxin 11a	PEX11a	AT1G47750		X	X
Peroxin 11d	PEX11d	AT2G45740		X	X
Dynamin-related protein 5B	DRP5B #	AT3G19720		X	
Peroxin 11b	PEX11b	AT3G47430		X	X
Peroxin 11e	PEX11e	AT3G61070		X	X
Peroxin 14	PEX14	AT5G62810		X	X
Chaperone					
α-Crystallin domain containing protein of 31.2 kDa	Acd31.2	AT1G06460	RLx_5HF/PKL	X	X
Methylglyoxal detoxification					
Glyoxylase I homolog	GLX1	AT1G11840			X
NADH/NADPH metabolism					
Glyceraldehyde-3-phosphate dehydrogenase C2	GAPC2	AT1G13440	SKA	X	X
NADP-dependent isocitrate deshydrogenase	ICDH	AT1G54340	SRL	X	X
Phosphogluconate dehydrogenase 2	6PGDH/ PGD2	AT3G02360	SKI	X	X
ROS detoxification					
Dehydroascorbate reductase 1	DHAR1	AT1G19570		X	X
Catalase 3	CAT3	AT1G20620	QKL(internal)	X	X
Catalase 1	CAT1	AT1G20630	QKL(internal)	X	X
Glutathione reductase 1	GR1	AT3G24170	TNL	X	

(Continued)

Table 1. Continued

Pathway/annotation	Symbol	At locus	PTS1/2	Protein identification T1	Protein identification T2
Monodehydroascorbate reductase 4	MDAR4	AT3G27820		X	X
Monodehydroascorbate reductase 1	MDAR1	AT3G52880	AKI		X
Glutathione S-transferase lambda 2	GSTL2 # $	AT3G55040	ARL		X
Ascorbate peroxidase 3	APX3	AT4G35000		X	X
Catalase 2	CAT2	AT4G35090	QKL(internal)	X	X
Ascorbate peroxidase 5	APX5 $	AT4G35970			X
Copper/zinc superoxide dismutase 3	CSD3	AT5G18100	AKL	X	X
Glutathione S-transferase theta 1	GSTT1	AT5G41210	SKI	X	X
Glutathione S-transferase theta 3	GSTT3 #	AT5G41220	SKM		X
Phylloquinone synthesis					
DHNA-CoA thioesterase 1	DHNAT1	AT1G48320	AKL	X	X
Naphthoate synthase	NS	AT1G60550	RLx$_5$HL	X	X
Pseudouridine catabolism					
Indigoidine synthase A	IndA	AT1G50510	RIx$_5$HL	X	X
Urate degradation					
Uricase	Uri	AT2G26230	SKL	X	X
Transthyretin-like protein 1	TLP1	AT5G58220	RLx$_5$HL	X	X
Transporter					
Peroxisomal NAD^+ carrier	PXN	AT2G39970		X	X
Peroxisomal membrane protein of 22kDa	PMP22	AT4G04470			X
Peroxisomal ABC transporter 1	PXA1	AT4G39850		X	X
Peroxisomal adenine nucleotide carrier 2	PNC2	AT5G27520		X	
Protease					
Peptidase family M16	PM16	AT2G41790	PKL	X	X
Lon protease homolog 2	Lon2	AT5G47040	SKL	X	X
Polyamine oxidation					
Copper amine oxidase	CuAO3	AT2G42490	SKL	X	X
Betaine aldehyde dehydrogenase	BADH	AT3G48170	SKL	X	X
Glyoxylate cycle					
Citrate synthase 3	CSY3	AT2G42790	RLx$_5$HL/SSV	X	X
Citrate synthase 2	CSY2	AT3G58750	RLx$_5$HL/SAL	X	X
Sulfite oxidation					
Sulfite oxidase	SO	AT3G01910	SNL	X	X
Nucleotide homeostasis					
Histidine triad family protein 3	HIT3	AT3G56490	RVx$_5$HF	X	X
Nucleoside diphosphate kinase type 1	NDPK1	AT4G09320			X
Histidine triad family protein 1	HIT1	AT4G16566	SKV		X
Histidine triad family protein 3	HIT2	AT5G48545	RLx5HL	X	X
Mevalonic acid (MVA) pathway					

(Continued)

Table 1. Continued

Pathway/annotation	Symbol	At locus	PTS1/2	Protein identification T1	Protein identification T2
Isopentenyl Diphosphate Isomerase 2	IPI2 #	AT3G02780			X
Amino acid metabolism					
Aspartate aminotransferase	ASP3	AT5G11520	RIx_5HL	X	X
Cobalamin-independent methionine synthase	ATMS1	AT5G17920	SAK	X	X
3-hydroxyisobutyryl-CoA hydrolase	CHY1	AT5G65940	AKL	X	X
Other or unknown functions					
Unknown protein 6	UP6	AT1G16730	SKL		X
Acetyl transferase 1	ATF1	AT1G21770	SSI		X
NADH: quinone reductase	NQR	AT1G49670	SRL	X	X
TSK-associating protein 1	TSA1 $	AT1G52410	SSL	X	X
GAST1 protein homolog 1	GASA1 ?	AT1G75750		X	X
Dehydrin family protein	ERD14 ? #	AT1G76180			X
Acetyltransferase 2	ATF2	AT1G77540	SSI		X
Glycine-rich protein 3	GRP3 ? #	AT2G05520			X
Unknown protein 3	UP3	AT2G31670	SSL	X	X
Harmless to ozone layer 3	HOL3 $	AT2G43940	STL	X	X
Senescence-associated protein/ B12D-related protein	B12D1	AT3G48140			X
Macrophage migration inhibitory factor 1	MIF1	AT3G51660	SKL	X	X
Zinc-binding dehydrogenase	ZnDH	AT3G56460	SKL	X	X
Unknown protein 5	UP5	AT5G44250	SRL	X	X

# indicates proteins identified for the first time in peroxisome proteomics. $ indicates proteins verified to be peroxisomal by *in vivo* targeting analysis. ? indicates proteins reported to be peroxisomal by (Cutler et al. 2000), but sequence information and microscopic images were not presented in this large-scale work thus need further confirmations.

stress-related functions; and (iii) having been detected in previous peroxisome proteomic studies but not confirmed by an independent approach (Table 2).

The yellow fluorescent protein (YFP) was fused to the N-terminus of each candidate protein to allow subcellular targeting functionality of the C-terminal PTS1. Through Agrobacterium-mediated transformation, each fluorescently-tagged candidate gene was transiently co-expressed with a fusion between the cyan fluorescent protein gene and the PTS1 tripeptide SKL (*CFP-PTS1*) in tobacco (*Nicotiana tabacum*) leaves. In some cases, we also co-expressed YFP tagged candidate genes with the mitochondrial marker gene *COX4-CFP* for further clarification. Two days later, tobacco leaf epidermal and/or mesophyll cells were subjected to confocal microscopy. In total, we confirmed the peroxisomal localization for six candidate proteins (Figures 2–5; Table 2).

Five of the confirmed proteins, i.e., hydroxy-acid oxidase 1 (HAOX1), glutathione S-transferase lambda 2 (GSTL2), short-chain dehydrogenase-reductase isoform e (SDRe), harmless to ozone layer 3 (HOL3), and TSK-associating protein 1 (TSA1), contained either a PTS1 or PTS1-like sequence (Table 2). SML> of HAOX1, ARL> of GSTL2, and SSL> of SDRe are well-established PTS1 tripeptides, and the YFP fusions of these proteins showed strong and almost exclusive localization to peroxisomes (Figure 2).

Harmless to Ozone Layer 3 (HOL3) has a C-terminal tripeptide STL> that was previously shown to be a functional PTS1 in an EST of glycolate oxidase (GOX) from *Catharanthus roseus* (Lingner et al. 2011), but not identified in any established *Arabidopsis* peroxisomal protein. YFP-HOL3 exhibited strong targeting to peroxisomes, while some YFP fluorescence also remained in the cytosol (Figure 3A). Since HOL3 has been

Table 2. Summary of *in vivo* targeting analyses

Annotation	Symbol	AT locus	PTS	Previous peroxisome proteome work	YFP-protein	Protein-YFP
Hydroxy-acid oxidase 1	HAOX1	AT3G14130	SML		Per	–
Glutathione S-transferase lambda 2	GSTL2	AT3G55040	ARL		Per	–
Short-chain dehydrogenase-reductase isoform e	SDRe	AT3G55310	SSL		Per	–
Harmless to ozone layer 3	HOL3	AT2G43940	STL	E2008; R2009	Cyt, per	–
Glutathione S-transferase TAU 20	GSTU20	AT1G78370		R2009	Cyt	Cyt
DEAD-box ATP-dependent RNA helicase 37	RH37	AT2G42520		R2007;2009	Cyt; vesicles	Cyt; vesicles
Glycine rich protein 2	GRP2	AT4G38680		Q2013	Cyt; vesicles	–
Ascorbate peroxidase 5	APX5	AT4G35970		E2008	Per; mito; chpt	–
Glyoxalase 2-3	GLX2-3	AT1G53580			Cyt	Mito
Ascorbate peroxidase 2	APX2	AT3G09640	RGx5HC		Cyt	Cyt
RING-H2 finger protein ATL65/ATL gene family member	ATL65	AT3G18930			Cyt	Vesicles; chpt
Alpha/beta-Hydrolases superfamily protein	–	AT3G47560			Cyt	cyt
3-Oxoacyl-[acyl-carrier-protein] reductase like protein 1	OARP1	AT4G20760			Dots	Mito; chpt
6-Phosphogluconolactonase 4	PGL4	AT5G24410			Cyt; vesicles	–
Fructose-bisphosphate aldolase 1, splicing isoform 2	FBA1.2	AT2G21330.2	SFL		Cyt	Chpt; mito
Glutamate-1-semialdehyde 2,1-aminomutase 1	GSA1	AT5G63570	SRI		Cyt	–
Aconitase 3	ACO3	AT2G05710	SKQ	E2008;R2009;Q2013	Cyt	Mito; chpt
60S ribosomal protein L19-1	RPL19A	AT1G02780	SKK		Cyt	–
TSK-associating protein 1	TSA1	AT1G52410	SSL	R2007;2009	Per	–

E2008, Eubel et al. 2008; R2007/2009, Reumann et al. 2007/2009; Q2013, Quan et al. 2013.

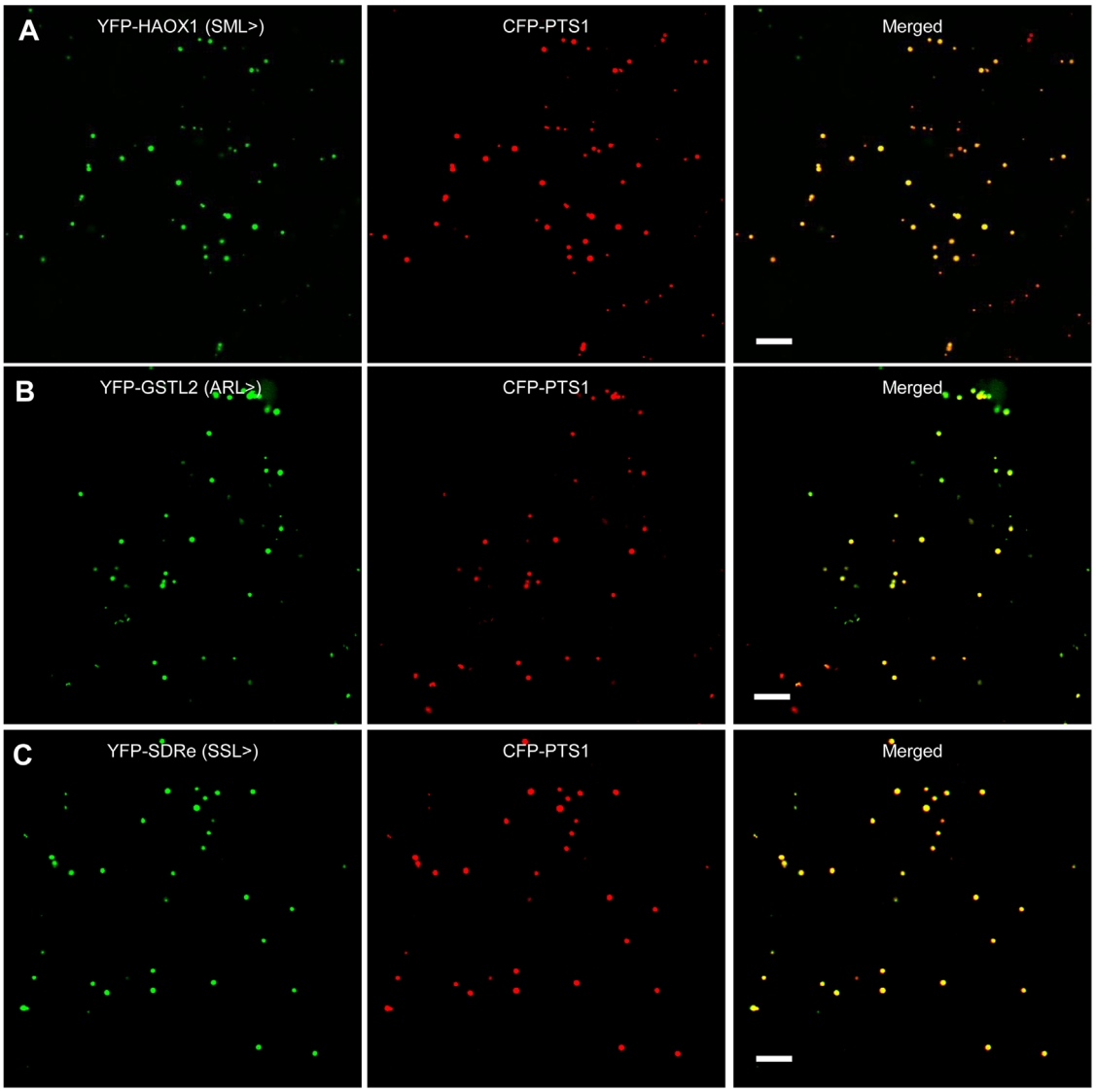

Figure 2. Peroxisome localization of HAOX1, GSTL2 and SDRe
Confocal images of the peroxisome localization of YFP-HAOX1 **(A)**, YFP-GSTL2 **(B)**, and YFP-SDRe **(C)** were taken in tobacco leaf epidermal cells transiently co-expressing each YFP fusion gene and the peroxisome marker *CFP-PTS1*. Scale bars = 10 μm. Predicted PTS1 tripeptides are shown in parentheses.

implicated in pathogen defense, we further investigated whether HOL3 was also peroxisomal in standard expression systems independent of Agrobacterium-mediated transformation. Indeed, YFP-HOL3 targeted to peroxisomes in both *Arabidopsis* protoplasts and onion epidermal cells (Figure 3B, C). Only few proteins with non-canonical PTS1 tripeptides, such as STL>, are peroxisomal because their peroxisome-targeting ability generally depends strongly on specific targeting-enhancing upstream residues (Lingner et al. 2011). Therefore, we also made fusions between the C-terminal 10 aa of HOL3 and YFP and showed that this decapeptide was sufficient to direct YFP to peroxisomes in both protein expression systems (Figure 3D, E). These results confirmed that STL> is a functional PTS1 and established HOL3 as the first *Arabidopsis* peroxisomal protein identified thus far that uses STL> as a PTS1.

TSA1 had not been reported to have any function associated with the peroxisome despite having an established but non-canonical PTS1, SSL>. Interestingly, YFP-TSA1, which contained the C-terminal 259 aa of the

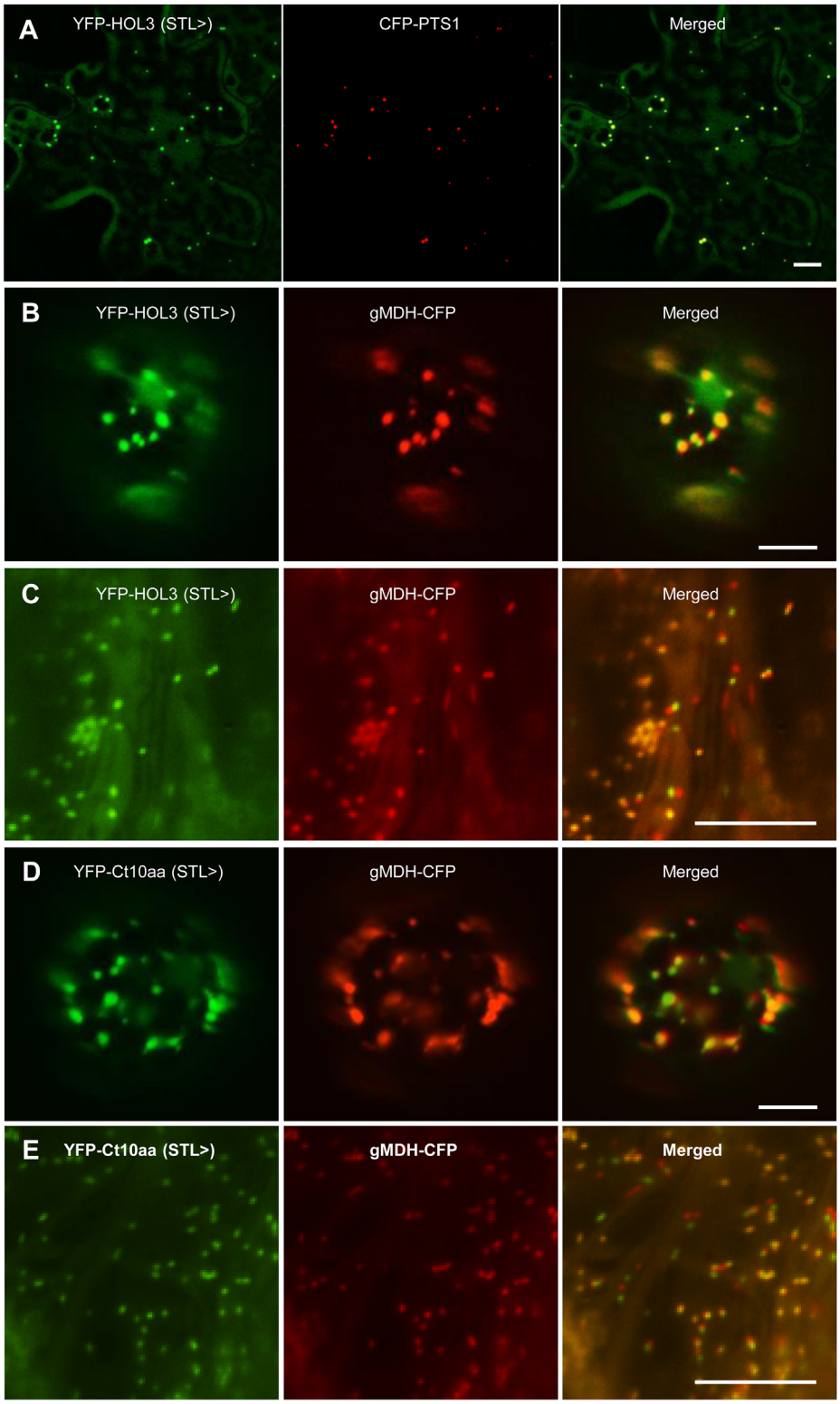

Figure 3. Peroxisome localization of YFP-HOL3 in three plant protein expression systems

(A) Confocal images of the peroxisome localization of YFP-HOL3 in tobacco leaf epidermal cells co-expressing *YFP-HOL3* and the peroxisomal marker *CFP-PTS1*. **(B–E)** Epifluorescence images of the peroxisome localization of YFP-HOL3 and YFP-Ct10aa (C-terminal 10 aa of HOL3) taken in *Arabidopsis* leaf protoplasts **(B, D)** and onion epidermal cells **(C, E)** that were transiently co-expressing each YFP fusion gene and the peroxisome marker *gMDH-CFP*. Scale bars = 10 μm. Predicted PTS1 tripeptides are shown in parentheses.

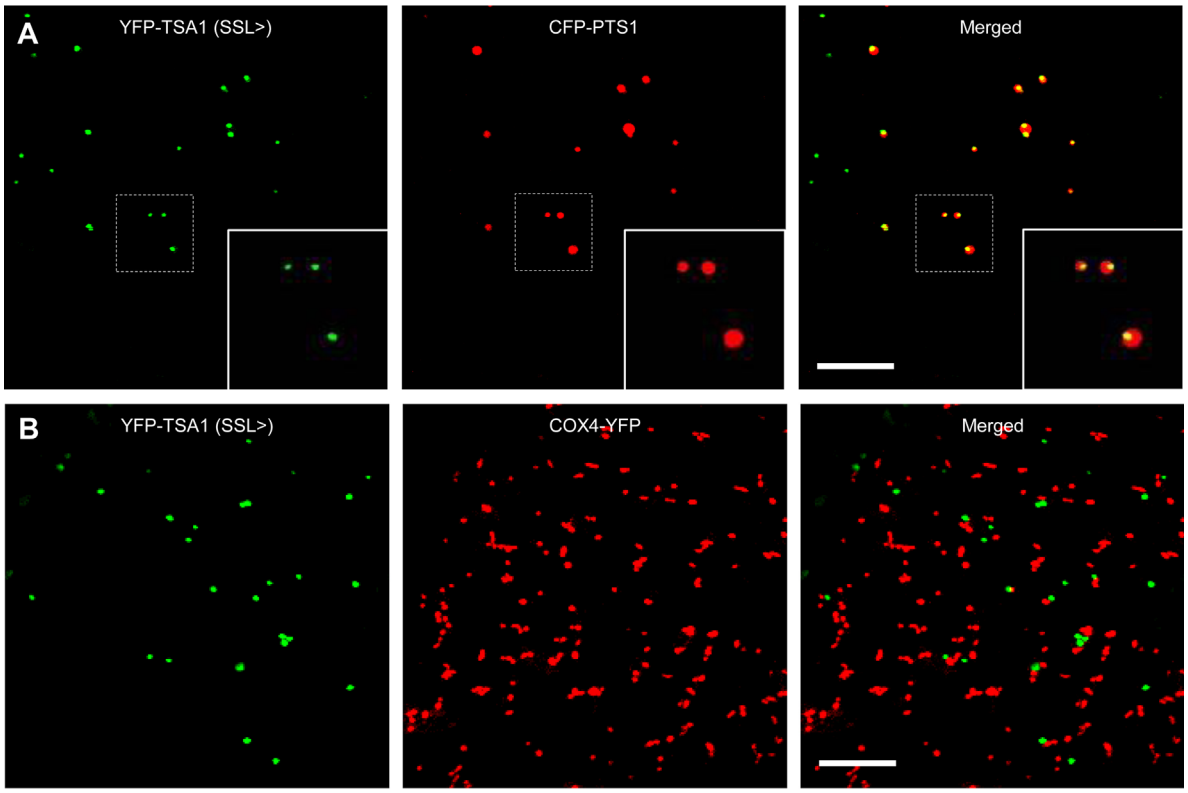

Figure 4. TSA1 is associated with peroxisomes
Confocal images of tobacco leaf epidermal cells transiently co-expressing *YFP-TSA1* (C-terminal 259 aa) and the peroxisome marker *CFP-PTS1* (**A**) or the mitochondrial marker *COX4-CFP* (**B**). Scale bars = 10 μm. Predicted PTS1 tripeptides are shown in parentheses. Insets in (**A**) are enlarged images of the boxed areas.

759 aa protein, was detected in small punctate structures that partially overlapped with the peroxisome matrix-localized marker protein, CFP-PTS1 (Figure 4A). This was not a random targeting pattern, because the protein had no association with other organelle markers, such as the mitochondrial marker COX4-CFP (Figure 4B). We speculated that TSA1 may not be imported into the peroxisome matrix, but instead is attached to the surface of peroxisomes.

As a paralog of the peroxisomal membrane protein APX3 (Narendra et al. 2006), APX5 also contains a predicted transmembrane domain (TMD) near its C-terminus, suggesting that it might be a C-terminal tail-anchored membrane protein like APX3. Consistent with this prediction, YFP-APX5 formed a ring structure surrounding the peroxisomal matrix (Figure 5A, B), suggesting that it is located on the membrane. Interestingly, YFP-APX5 fluorescence was also detected on the chloroplast outer-membrane (Figure 5C). Furthermore, YFP-APX5 showed strong signals overlapping with mitochondria (Figure 5D) and when examined at higher magnification, was seen to, at times, form a ring structure (Figure 5E), suggesting that it is also localized to one of the two mitochondrial membranes.

Confocal microscopic analysis did not detect peroxisomal association for the other 13 candidate proteins (Table 2). Among them, GSA1 (SRI>), FBA1.2 (SFL>), RPL19A (SKK>) and ACO3 (SKQ>) contained PTS1 or PTS1-like peptides (Table 2), yet their N-terminally tagged YFP fusions were all observed to be cytosolic (Figures S2A, S2B, S3A, S4A). Glutathione S-transferase TAU 20 (GSTU20), DEAD-box ATP-dependent RNA helicase 37 (RH37) and glycine rich protein 2 (GRP2) do not have PTS-related peptides but were detected in previous peroxisome proteome studies and this study (Table 2). YFP-GSTU20 was cytosolic (Figure S4C), and both YFP-RH37 and YFP-GRP2 were detected in the cytosol as well as in small vesicle-like structures that were neither peroxisomal nor mitochondrial (Figures S5A, S6A).

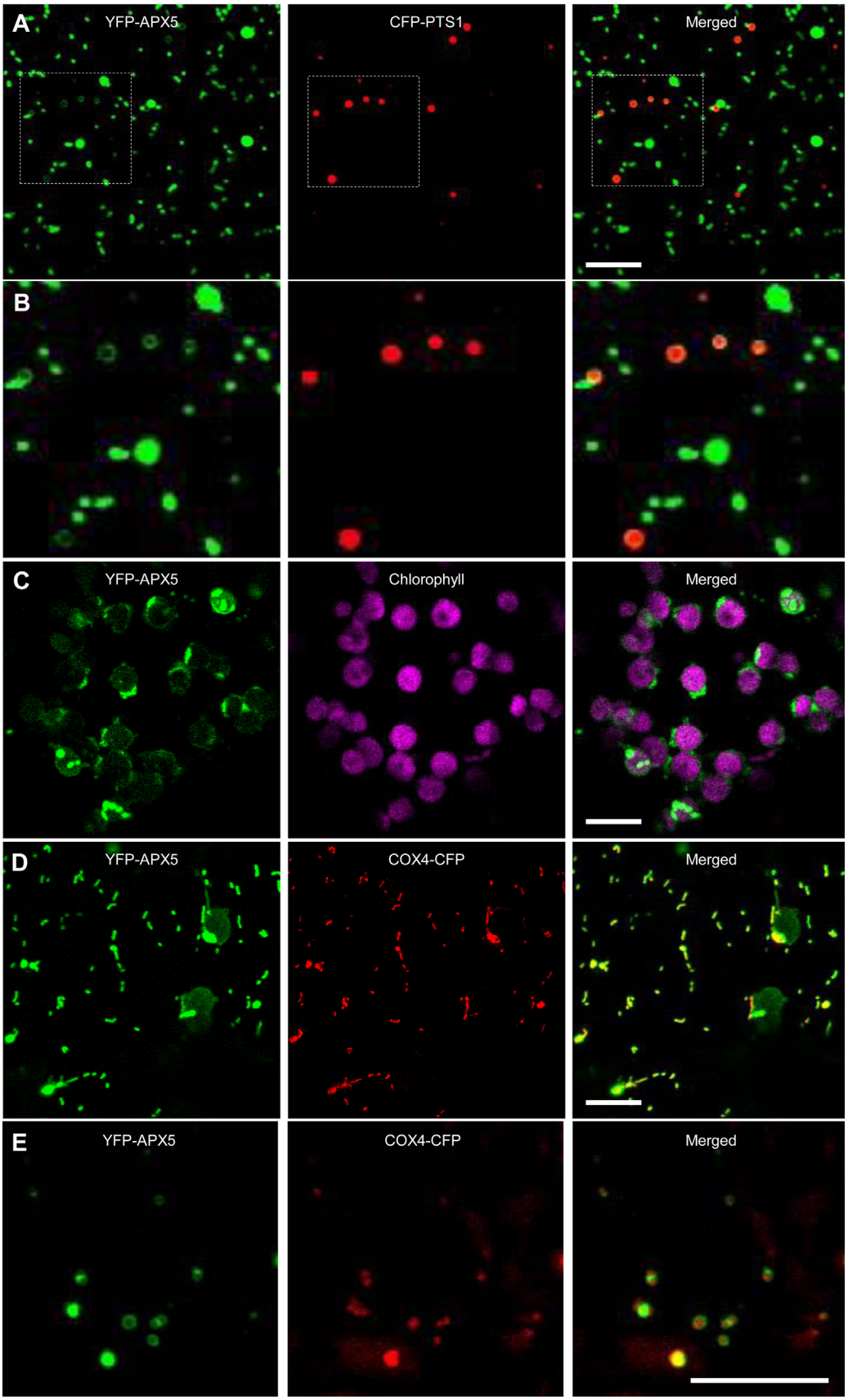

Figure 5. Continued

The remaining six proteins tested lacked PTS1-related peptides, but were specifically detected in this peroxisome proteomic study and had possible links with peroxisomes based on annotation or predicted functional domains. These included glyoxalase 2-3 (GLX2-3) presumably involved in methylglyoxal catabolism together with peroxisomal GLX1 (Reumann et al. 2009; Quan et al. 2010), ascorbate peroxidase 2 (APX2) that participates in ROS degradation, and the RING-H2 finger E3 ubiquitin ligase ATL65 (an *Arabidopsis* Tóxicos en Levadura protein family member) implicated in protein ubiquitination/degradation. In addition, the alpha/beta-hydrolases superfamily protein AT3G47560 and 3-oxoacyl-[acyl-carrier-protein] reductase like protein 1 (OARP1) were implicated in fatty acid metabolism, and 6-phosphogluconolactonase 4 (PGL4) belongs to the oxidative pentose phosphate pathway. YFP-GLX2-3, YFP-APX2, YFP-ATL65 and YFP-AT3G47560 localized to the cytosol (Figures S6B, S7A, S8A, S9A), YFP-PGL4 was mainly cytosolic but was also localized to small vesicle-like structures that were not associated with the peroxisomal or mitochondrial marker (Figure S9C), and YFP-OARP1 localized to vesicle-like structures that were neither peroxisomes nor mitochondria (Figure S10A).

Out of the 13 candidates that did not show peroxisome association as N-terminal YFP fusions, APX2 contained a PTS2-like peptide RGx_5HC, and GSTU20, RH37, FBA1.2, ACO3, GLX2-3, ATL65, AT3G47560 and OARP1 contained putative N-terminal chloroplast transit peptides, mitochondrial targeting signals or signal peptides for the secretory pathway, as predicted by the TargetP 1.1 Server (http://www.cbs.dtu.dk/services/TargetP/). Therefore, C-terminal YFP fusion proteins were also created for these nine proteins and assessed for subcellular localization (Table 2); none were observed to be associated with peroxisomes. FBA1.2-YFP localized to chloroplasts in all cells and to mitochondria in some cells (Figure S2C), ACO3-YFP targeted strongly to both chloroplasts and mitochondria (Figure S3B), GLX2-3-YFP was mitochondrial (Figure S6C), and OARP1-YFP was dual-targeted to mitochondria (in all cells) and chloroplasts (in some cells; Figure S10B). Cytosolic localization was observed for GSTU20-YFP (Figure S4D), APX2-YFP (Figure S7B) and AT3G47560-YFP (Figure S9B). RH37-YFP was cytosolic and in punctate structures that did not overlap with peroxisomes or mitochondria (Figure S5B). ATL65-YFP localized to vesicle-like structures that did not overlap with peroxisomes or mitochondria but appeared to be associated with chloroplasts (Figure S8B).

High coverage of peroxisomal proteins

Together with the six newly verified peroxisomal proteins, the number of authentic peroxisomal proteins identified in this study was 111 (Table 1), which is higher than those identified from any previously reported peroxisome proteomic study. Using normalized spectral abundance factors (NSAFs) to represent the actual abundance of identified proteins (Paoletti et al. 2006), we determined the enrichment of peroxisomal proteins in the total identified proteins to be 76% in T1 and 80% in T2 in protein abundance (Figure 6A). The enrichment of peroxisomal proteins in this proteomic study is comparable to those in our two previous studies using *Arabidopsis* green leaves (~75%) and etiolated seedlings (~65%) (Reumann et al. 2009; Quan et al. 2013).

All identified proteins were divided into groups based on their relative abundance (NSAF) in the isolated peroxisome fraction. Proteins with very high abundance ($NSAF > 0.025$) were all peroxisomal, whereas non-peroxisomal proteins became prevalent as protein abundance decreased (Figure 6B). However, many peroxisomal proteins were still present in the low abundance range. For example, out of the six proteins validated to be peroxisomal in this study, five had very low abundance ($NSAF < 0.0002$), and HOL3 had relatively low abundance ($NSAF < 0.0007$), demonstrating the importance of analyzing the low abundance range to discover novel peroxisomal proteins.

Figure 5. APX5 localizes to peroxisomes, chloroplasts and mitochondria

Confocal images of tobacco leaf epidermal cells transiently co-expressing *YFP-APX5* and the peroxisome marker *CFP-PTS1* (**A, B**), leaf mesophyll cells transiently expressing *YFP-APX5* alone (**C**), or leaf epidermal cells transiently co-expressing *YFP-APX5* and the mitochondrial marker *COX4-CFP* (**D, E**). Scale bars = 10 μm. (**B**) Enlarged images of the boxed areas in (**A**).

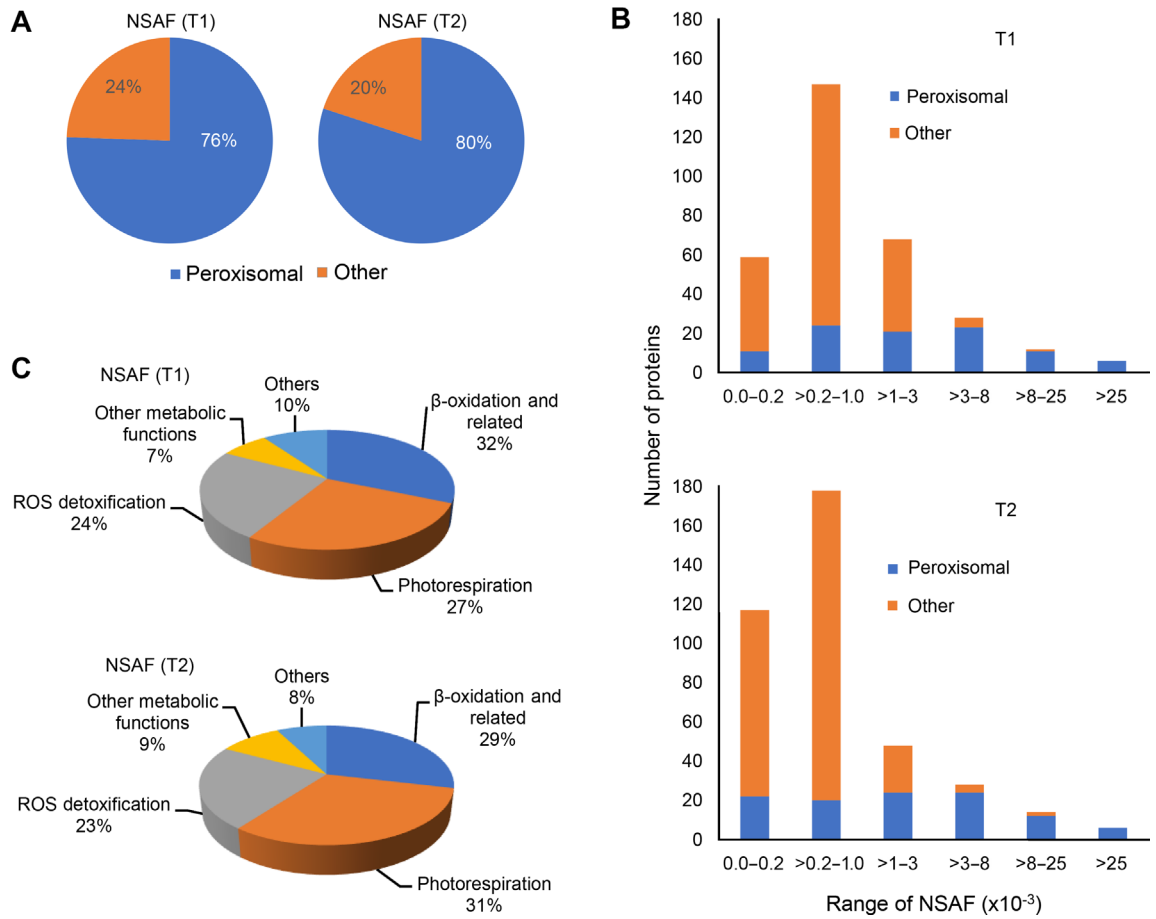

Figure 6. Abundance and functions of peroxisomal proteins identified in this study

(A) Relative abundance (NSAF) of peroxisomal proteins identified in this study. T1 and T2 represent the two pools of peroxisome preparations Total 1 and Total 2. **(B)** Classification of peroxisome-associated proteins and other proteins identified in this study, based on relative abundance (NSAF). **(C)** Functional categorization of peroxisomal proteins shown by percentage of relative abundance (NSAF). The category of 'β-oxidation and related' includes proteins involved in core β-oxidation, auxiliary β-oxidation, JA biosynthesis, IBA biosynthesis, lipid catabolism and acyl-CoA hydrolysis, as shown in Table 1. The category of 'other metabolic functions' includes protein involved in methylglyoxal detoxification, phylloquinone synthesis, pseudouridine catabolism, urate degradation, polyamine oxidation, sulfite oxidation, glyoxylate cycle, mevalonic acid (MVA) pathway and amino acid metabolism, as shown in Table 1. The 'others' category includes proteins involved in peroxisome biogenesis, NADH/NADPH metabolism, nucleotide homeostasis and transporters, proteases, chaperones, and other proteins of unknown functions, as shown in Table 1.

The abundance of peroxisomal proteins in major functional categories was further analyzed. The relative abundance of photorespiration-related proteins was 27%–31% (Figure 6C), which was lower than the approximately 45% in green leaves (same plant age) in our previous study (Reumann et al. 2009). In contrast, the abundance of ROS detoxification-related proteins was 23%–24% (Figure 6C), much higher than the approximately 15% in green leaves (Reumann et al. 2009). The abundance of proteins related to β-oxidation was comparable to green leaves (Reumann et al. 2009). These data are consistent with the notion that during senescence photosynthesis is reduced, whereas ROS detoxification is increased.

Proteome comparison of peroxisomes under three different conditions

Peroxisomal metabolic pathways vary both quantitatively and qualitatively between tissue types, as shown in our previous peroxisomal proteome studies of green

leaves and etiolated seedlings (Reumann et al. 2009; Quan et al. 2013). Although there were some differences in protein quantity and fractionation methods, and versions of the *Arabidopsis* database used for protein identification, these three datasets were developed by our group, using the same method for peroxisome isolation and same mass-spec device and settings for protein identification. Therefore, we used these datasets to conduct a general comparison of protein constituents and metabolic pathways in peroxisomes in etiolated seedlings, green leaves and dark-induced senescent leaves.

Collectively, these three studies detected 125 peroxisomal proteins (Figure 7; Table S4). Sixty-seven of these proteins were shared by all three datasets, covering major peroxisomal biochemical processes, such as β-oxidation, hormone biosynthesis, photorespiration, and ROS detoxification (Table S4). Thirty-two proteins were shared only between peroxisomes of green leaves and dark-treated senescent leaves (Figure 7; Table S4). From peroxisomes of dark-treated leaves, we identified, to our knowledge, all previously established peroxisomal proteins involved in ROS detoxification, except for one (GSTT2). These included all three catalase isoforms (CAT1, CAT2 and CAT3), all enzymes in the ascorbate-glutathione cycle (APX3, DHAR1, GR1, MDAR1 and MDAR4), two GSTs of the theta class (GSTT1 and GSTT3), and copper/zinc superoxide dismutase isoform 3 (CSD3) (reviewed in Pan and Hu 2018), in addition to the newly confirmed GSTL2 and APX5. Among them, CAT1 to 3, CSD3 and APX3–enzymes directly degrading ROS – were detected in all three proteomes. In contrast, dehydroascorbate reductase 1 (DHAR1), monohydroascorbate reductase 4 (MDAR4), monohydroascorbate reductase 1 (MDAR1) and glutathione reductase 1 (GR1) – the three reductases involved in the regeneration of ascorbate and glutathione in the glutathione/ascorbate cycle, were only shared by the two leaf types (Table S4).

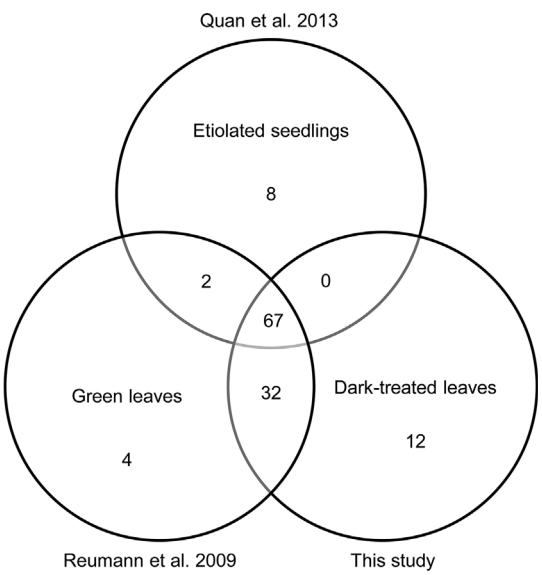

Figure 7. A Venn diagram comparing the number of peroxisomal proteins identified from three proteomic studies using different tissues

Members of some protein families, such as acyl-activating enzyme (AAE), acyl-CoA oxidase (ACX), 3-ketoacyl-CoA thiolase (KAT), peroxin 11 (PEX11), small thioesterase (ST), and histidine triad family protein (HIT), were shared by all three proteomes, or by the two types of leaves (Table S4). No proteins were shown to be in common only between etiolated seedlings and senescent leaves, and only GOX2 and GOX3 were found to be in common exclusively between peroxisomes from etiolated seedlings and green leaves (Figure 7), consistent with the fact that etiolated seedlings differ substantially from leaves in their physiology.

Eight proteins, including isocitrate lyase (ICL), malate synthase (MLS), a small heat shock protein Hsp15.7, acetoacetyl-CoA thiolase 1.3 (AACT1.3), benzoyloxyglucosinolate 1 (BZO1), response to drought 21A-like 1 (RDL1), serine carboxypeptidase-like protein 20 (SCPL20), and unknown protein 9 (UP9), were only detected in etiolated seedlings (Table S4). This is consistent with the fact that ICL and MLS are major enzymes in the glyoxylate cycle, which occurs predominantly in peroxisomes within seeds/fatty tissue and germinating seedlings, and is tightly related to core β-oxidation through its generation of acetyl-CoA (Beevers 1979). The higher number of proteolytic enzymes in seedling peroxisomes might reflect the fact that some glyoxysome-specific enzymes are being degraded as seedlings prepare for photorespiration.

The four proteins specifically detected in peroxisomes of green leaves were dephospho-CoA kinase (CoAE), malonyl-CoA decarboxylase (MCD), esterase/lipase/thioesterase family 1 (ELT1) and Unknown protein 7 (UP7). The physiological functions of these proteins are not well defined, and whether or not the related biochemical functions are more active in green leaves remains to be determined.

The largest group of peroxisomal proteins detected specifically in one type of tissue was the 12 proteins uniquely detected in peroxisomes from dark-treated senescent leaves (Table S4). These included HAOX1, SDRe, acyl CoA thioesterase family protein (ACH), dynamin-related protein 5B (DRP5B), GSTL2, APX5, glutathione S-transferase theta 3 (GSTT3), peroxisomal membrane protein of 22 kDa (PMP22), peroxisomal adenine nucleotide carrier 2 (PNC2), isopentenyl diphosphate isomerase 2 (IPI2), glycine-rich protein 3 (GRP2), and early response to dehydration 14 (ERD14), most of which belong to protein families for which other members were detected in the other two proteome studies (Table S4). DRP5B, a dynamin-related protein shared by the division of peroxisomes and chloroplasts, was detected for the first time in a peroxisome proteome study (Table S4). According to the online database *Arabidopsis* eFP browser (http://bar.utoronto.ca/; Winter et al. 2007), seven of these 12 genes (*HAOX1*, *SDRe*, *ACH*, *GSTT3*, *PMP22*, *PNC2* and *ERD14*) exhibited various levels of increased expression in senescent leaves in comparison with green leaves (Figure S11), indicating that their protein products may play a more important role under senescent conditions.

DISCUSSION

Identification of a large number of peroxisomal proteins

This study detected the highest number of peroxisomal proteins among all reported peroxisome proteome studies, across various organisms. We identified 111 peroxisomal proteins, including 105 previously established and six newly identified and verified. The two previous proteome studies of *Arabidopsis* peroxisomes, reported by our group, identified 80 peroxisomal proteins (including 15 new ones) from green leaves and 77 (including 11 new ones) from etiolated seedlings (Reumann et al. 2009; Quan et al. 2013). The number of peroxisome proteins detected in other previous peroxisome proteome studies in plants ranged from approximately 20 to approximately 90 (Fukao et al. 2002, 2003; Reumann et al. 2007; Arai et al. 2008; Eubel et al. 2008). Interestingly, peroxisome proteome studies in non-plant systems generally identified fewer proteins than those in plants despite advanced quantitative proteome methodologies (Mi et al. 2007; Wiederhold et al. 2010; Gronemeyer et al. 2013). This suggests that plant peroxisomes may exceed fungal and animal peroxisomes in terms of metabolic capability, flexibility and functional subtype specialization.

In this study, we identified six additional peroxisomal proteins, indicating that additional novel peroxisomal proteins will likely be identified through experiments conducted on plants exposed to various environmental and physiological conditions. The use of a stress condition in this study also likely increased the probability for identifying new peroxisomal proteins. Some candidate proteins failed to localize to peroxisomes in our *in vivo* targeting analysis, but whether any of these proteins display peroxisomal targeting exclusively under senescence and/or dark conditions needs further investigation. Finally, it is also possible that some peroxisomal proteins that function specifically in peroxisomes during senescence were not identified, as a 48 h dark treatment may have been too short to induce some metabolic processes involved in senescence.

New peroxisomal proteins potentially involved in fatty acid catabolism and ROS detoxification

HAOX1 and its close homolog HAOX2 are members of the L-2-hydroxy acid oxidase family, which contains three other well-known peroxisome-localized members, namely GOX1/2/3 (Reumann et al. 2004; Esser et al. 2014). GOX1 and GOX2 have major functions in photorespiration, whereas GOX3 converts L-lactate to pyruvate and possibly functions to keep L-lactate at low levels (Reumann et al. 2004; Engqvist et al. 2015). Recombinant HAOX1 produced in *E. coli* exhibited highest activity with 2-hydroxydodecanoic acid, whereas HAOX2 had highest activity for leucic acid, and both HAOXs displayed low activity with glycolate, suggesting that they likely participate in fatty acid and protein catabolism rather than photorespiration (Esser et al. 2014). HAOX2 was earlier identified in leaf peroxisomes and confirmed by fluorescence microscopy (Reumann et al. 2009). The *in vivo* metabolic roles of HAOX1 and HAOX2 and their physiological importance remains to be established.

As a member of the short-chain dehydrogenases/reductases (SDR) protein family, the newly identified SDRe shares 95% amino acid identity with the peroxisomal SDRd protein (At3g55290) (Reumann et al. 2007,

2009; Eubel et al. 2008; Quan et al. 2013). SDRe and SDRd share approximately 34% and approximately 29% amino acid sequence identity, respectively, with human mitochondrial 17beta-hydroxysteroid dehydrogenase type 8 (HSD17B8) (Ohno et al. 2008; Chen et al. 2009) and peroxisomal trans-2-enoyl-CoA reductase (PECR) (Gloerich et al. 2006). It will be interesting to study the predicted reductase function of SDRd and SDRe toward specific fatty acids and their derivatives and the possible relationship to auxiliary β-oxidation.

The finding of a higher number of proteins involved in ROS metabolism in these peroxisomes is consistent with previous reports that described active metabolism of ROS, nitric oxide and NADPH in peroxisomes from senescent pea plants (Pastori and del Rio 1997; Corpas et al. 1999; 2004). GSTL2 belongs to the lambda class of the *Arabidopsis* glutathione transferase (GST) superfamily, whose members are components of cellular detoxification systems and have the ability to conjugate reduced glutathione (GSH) to electrophilic substrates, such as peroxidized lipids and xenobiotics, for breakdown (Sheehan et al. 2001).

After removal of its putative chloroplast transit peptide at the N-terminus, GFP-GSTL2 was detected in both peroxisome-like punctate structures and the cytosol (Dixon et al. 2009). Our study provides the first report of GSTL2 in peroxisomes through proteomics, and further confirmed that YFP-GSTL2 (full-length) specifically targeted to peroxisomes (Figure 2B). Three GSTs of the theta class (GSTT1-3) were also shown to target peroxisome-like structures (Dixon et al. 2009). Previously, only GSTT1 had been identified by peroxisome proteome analyses (Reumann et al. 2007, 2009; Eubel et al. 2008; Quan et al. 2013). Here, we detected three peroxisomal GSTs (Table 1), suggesting that GSTT1 is constitutive, whereas the function of the other GSTs may be stress related. In addition to GSTL2 and APX5, we also identified all the peroxisomal proteins known to be involved in ROS detoxification (except GSTT2; Table 1), underscoring the key role of peroxisomal ROS degradation during senescence and dark-induced stress.

HOL3, the first *Arabidopsis* peroxisomal protein with a PTS1 STL>, is possibly involved in methyl halide production

HOL1 to 3 constitute a small subfamily of methyltransferases, and recombinant proteins of all three isoforms catalyze the S-adenosyl-L-methionine (SAM)-dependent methylation of halogenids to produce methyl halides *in vitro* (Nagatoshi and Nakamura 2007). It was reported that tropical and subtropical plants were the largest sources of methyl chloride (Yokouchl et al. 2002). Mutant analysis showed that the production of methyl halide is primarily controlled by HOL1 (Nagatoshi and Nakamura 2007). Physiologically, recombinant HOL1 was shown to be highly active in methylating thiocyanate (SCN^-), a product of glucosinolate breakdown upon tissue damage, resulted in CH_3SCN production that was correlated with a dramatic increase in *Arabidopsis* defense against phytopathogens (Nagatoshi and Nakamura 2009). HOL1 and HOL2 do not contain PTS-related peptides, and have not been identified in peroxisome proteome studies. In contrast, HOL3 contains an STL>, a rare and weak PTS1. Besides this study, HOL3 was detected in at least two previous peroxisome proteome studies (Eubel et al. 2008; Reumann et al. 2009). Thus, HOL3 is a specific peroxisomal methyl transferase that may have methylation-related functions towards a substrate generated in the peroxisomal matrix, and may have a function in pathogen defense.

APX5, a new peroxisomal antioxidant enzyme shared with mitochondria and chloroplasts

Having a higher affinity to H_2O_2 than catalase, peroxisomal APX functions in the ascorbate-glutathione cycle, a peroxisomal membrane-associated H_2O_2 detoxification system complementary to catalases (reviewed in Kaur and Hu 2009). Out of the eight APXs in *Arabidopsis*, only APX3 was previously shown to be peroxisomal by *in vivo* targeting analysis (Narendra et al. 2006), and was detected in multiple peroxisome proteome studies (Fukao et al. 2002, 2003; Reumann et al. 2007, 2009; Eubel et al. 2008; Quan et al. 2013). APX3 overexpression had various benefits, including increased tolerance and seed production during stress (reviewed in Kaur and Hu 2009). However, analysis of an *apx3* loss-of-function mutant established that APX3 was dispensable under normal and stress conditions, suggesting that it may be functionally redundant with other APX proteins (Narendra et al. 2006). APX5 shares the highest sequence similarity with APX3 among all *Arabidopsis* APXs (Panchuk et al. 2002), and was also detected in a peroxisome proteome study using *Arabidopsis* cell suspension culture subjected to a 7-d

dark treatment (Eubel et al. 2008), indicating that long-term darkness, or other stresses, may lead to an increase of APX5 in peroxisomes.

APX5 was shown to be associated with the mitochondrial outer membrane, by mitochondrial proteomics and *in vivo* targeting analysis using APX5-GFP (Duncan et al. 2011), but its chloroplast localization was unknown until this study. Peroxisomes, mitochondria and chloroplasts are three organelles with important functions in various aspects of energy metabolism, each hosting numerous ROS producing reactions and operate cooperatively in some metabolic pathways, such as photorespiration. The interesting triple localization pattern of APX5 needs to be further clarified, as APX5 appears to be a shared component of antioxidant systems in all three energy organelles. Consistent with these findings, increased APX activities were reported during leaf senescence in pea peroxisomes, mitochondria and chloroplasts (Jiménez et al. 1998; Palma et al. 2006; Ribeiro et al. 2017).

TSA1, a new peroxisomal protein potentially linking peroxisomes and the cytoskeleton

TSA1 was first shown to interact with TONSOKU (TSK), a protein with an important role in the maintenance of meristem organization and cell division (Suzuki et al. 2005). When transiently expressed in tobacco BY-2 cells, TSA1-GFP localized to small cytoplasmic vesicles and was suggested to play a role in mitosis (Suzuki et al. 2005). TSA1 was also identified as an interacting partner of CSN1, a subunit of the COP9 signalosome (CSN) involved in diverse cellular and developmental processes (Li et al. 2011). The *tsa1* mutants had short hypocotyls when germinated in darkness, suggesting that TSA1 may be involved in seedling development (Li et al. 2011).

TSA1 was also identified as an interacting partner of ã-TuC Protein 3-Interacting Protein 1 (GIP1), which is involved in the organization of microtubules (Batzenschlager et al. 2013). Moreover, TSA1-GFP was reported to partially localize to the nuclear envelope, where the interaction between TSA1 and GIP1 occurred, suggesting TSA1 might be part of the structural link between the nuclear envelope and the cytoskeleton (Batzenschlager et al. 2013). In these reports, TSA1-GFP fusions were used for subcellular localization, blocking its predicted PTS1 tripeptide. Here, we discovered a novel localization of TSA1 to peroxisomes by fusing YFP at its N-terminus. The partial overlap between YFP-TSA1 and peroxisomes, together with a potential role of TSA1 in microtubule organization, suggested a putative role of TSA1 in cytoskeleton-peroxisome connection. Previous peroxisome proteomic studies using green leaves of *Arabidopsis* also detected TSA1 (Reumann et al. 2007, 2009), indicating that its peroxisome association may not be specific to stress or senescence.

Towards a complete *Arabidopsis* peroxisomal proteome

Major obstacles for establishment of a complete catalog for the peroxisome proteome, based on proteome studies, include difficulties in detecting membrane and transient peroxisomal proteins. It is possible that some proteins are targeted to peroxisomes only under specific conditions, for example, during senescence, in detached leaves or after dark treatment. Such proteins could not be verified as peroxisomal in our *in vivo* subcellular targeting analyses using a transient expression system. In such cases, it would be necessary to obtain stable transgenic plants and analyze the localization of these proteins under specific conditions.

The possibility also exists that we mistakenly grouped some proteins into the list of contaminants and, hence, did not analyze their peroxisome association. Furthermore, some proteins lacking a PTS might be targeted to the peroxisome through the so-called piggyback transport, via their interaction with another peroxisomal protein that contains a PTS (reviewed in Hu et al. 2012). In this case, peroxisome targeting of these proteins would depend on their co-expression with a yet unknown "partner gene". Finally, although isoform-specific peptides were not detected for four previously established peroxisome proteins, namely GOX2, GOX3, ACX6 and GSTT2, to differentiate them from close paralogs for a positive identification (Table S1), these four proteins might have been detected in our study. Taken together, the actual number of peroxisomal proteins detected in this study could be even higher than the 111 we reported.

To comprehensively map the proteomes of all plant peroxisomal subtypes and to compare their protein constituents in different tissue types, other plant organs will need to be used. In addition to darkness, senescence can be induced by other means, such as ethylene treatment, and other types of stress could be

applied to the plant to discover peroxisomal proteins specifically involved in such stress responses.

MATERIALS AND METHODS

Plant growth, induction of senescence and isolation of peroxisomes from senescent leaves

Wild-type seeds of *Arabidopsis thaliana* ecotype Columbia-0 were grown in soil for 4 weeks, in a growth chamber, with a 16 h/8 h light/dark cycle and 100 to 150 μmol/m^2/s light. To induce uniform senescence, 4-week-old plants were detached from the primary root by one single cut (approximately 60 g FW per isolation) and collected in a large perforated tray housed in a second tray filled with water to a depth of approximately 0.5 cm. Styrofoam strips prevented the detached plants from making direct contact with the water. The trays were enclosed in plastic bag to maintain high humidity and prevent leaf wilting, and kept in the dark at room temperature for 48 h, at which chlorophyll degradation and leaf senescence became apparent.

Peroxisomes were isolated, as previously described (Reumann et al. 2007), with slight modifications. Briefly, twice the amount of protease inhibitors was used compared with green leaf peroxisome preparation because, in general, protease activity including that in peroxisomes, is increased during senescence (Distefano et al. 1999). Purity analysis of isolated peroxisomes was performed as previously described (Reumann et al. 2009).

Mass spectrometry analysis and protein identification

500 μg each of highly enriched peroxisomal proteins were loaded onto a single lane of an SDS-PAGE gel. The protein sample was run 2 cm into the resolving gel, which was then sliced into eight pieces. Proteins in each slice were *in-gel* digested by trypsin, and subjected to liquid chromatography-electrospray ionization-tandem mass spectrometry (LC-ESI-MS/MS), as previously described (Reumann et al. 2009). MS data analysis and determination of protein identification was performed, as previously described (Reumann et al. 2009), but with modifications in the software version (Scaffold 4), genome database version (TAIR10) and filtering threshold (1% false discovery rate for protein identification, minimal 1 peptide and 95% probability for peptide identification). A protein was determined to be identified if it had at least 99% probability for protein identification.

Gene cloning and plasmid construction

For subcellular targeting analysis using the tobacco system, gene amplification by PCR and plasmid construction, using the Gateway cloning technique, were performed as previously described (Pan et al. 2014, 2016). For gene cloning for protein targeting analysis using *Arabidopsis* protoplasts and onion epidermal cells, reporter gene constructs were generated as described previously (Lingner et al. 2011). Vectors and primers used in this study are given in Table S5.

Transient protein expression and *in vivo* targeting analysis

Transient protein expression in a tobacco leaf system followed by confocal microscopy to analyze protein targeting, was carried out as previously described (Pan et al. 2014, 2016).

For transient expression in *Arabidopsis* protoplasts, 2 to 4-week-old plants, which did not show any signs of stress or senescence [grown on soil, V.2.1.2, 10-15 young leaves (approximately 1 g)] were harvested for protoplast isolation. Leaves were cut with a sharp blade into small strips, and incubated overnight at room temperature in the dark with an enzyme solution [1.5% (w/v) cellulase R10, 0.4% (w/v) Macerozyme R10, 0.4 M Mannitol, 20 mmol/L KCl, 20 mmol/L MES pH 5.7, and 10 mmol/L $CaCl_2$, 0.1 % (w/v) BSA] to decompose the cell wall. On the next day, the protoplast suspension was filtered through a 63 μm mesh and protoplasts collected by centrifugation (100 *g* for 3 min at 18°C) and then resuspended in Solution D (154 mmol/L NaCl, 125 mmol/L $CaCl_2$, 5 mmol/L KCl, and 2 mmol/L MES pH 5.7), followed by protoplast counting, using a hemacytometer. For transformation, protoplasts were pelleted again and resuspended in Solution C (0.4 M Mannitol, 15 mmol/L $MgCl_2$, 4 mmol/L MES pH 5.7) to a final protoplast concentration of 2×10^5 cells/mL. Plasmid DNA (2.5 μg) was added to 125 μL of protoplast solution (2×10^5 cells/mL), followed by addition of 137.5 μL of Solution B [61.5% (w/v) PEG 4000, 0.3 M Mannitol, and 0.15 M $CaCl_2$] and then a 30 min incubation at RT. After incubation, protoplasts were collected by centrifugation and resuspended in 4 mL solution D, and incubated

overnight at RT, in the dark. The next day (18–24 h post transformation [pt]) the protoplast solution was centrifuged, and washed again with solution D. Microscopic analyses were carried out 18–48 h pt.

For protein transient expression in onion epidermal cells, gold particles (BioRad) were coated with recombinant genes of interest. Healthy onions were cut into slices, transferred to Petri dishes, and placed on a wet tissue paper. Onion slices were bombarded using a Biolistic Particle Delivery System (BioRad, USA) with rupture discs (1,100 psi) under vacuum of 0.1 bars. After transformation, samples were incubated overnight in darkness, and microscopic analyses were performed on the next day.

Fluorescence microscopy analyses of *Arabidopsis* protoplasts and onion epidermal cells was performed using a Nikon TE-2000U inverted fluorescence microscope equipped with an illumination system Exfo X-cite 120 (Excelitas Technologies, Waltham, USA). Different filters were used for YFP (exciter HQ500/20, emitter S535/30) and CFP (exciter D436/20, emitter D480/40). Images were captured by a Hamamatsu Orca ER 1394 cooled CCD camera. NIS-Elements Basic Research (Nikon, Tokyo, Japan) and Adobe Photoshop Elements were used for analysis and standard image acquisition.

ACKNOWLEDGEMENTS

We thank Danielle Holbrook for technical assistance in peroxisome isolation, and Doug Whitten of the Michigan State University proteomics facility for performing the LC-MS/MS analysis. This work was supported by grants from the National Science Foundation to J.H. (MCB 0618335; MCB 1330441) and L.J.O. (MCB 0618279).

AUTHOR CONTRIBUTIONS

R.P. analyzed the proteomics data, performed most of the *in vivo* targeting analyses, and drafted the manuscript. S.R. established leaf peroxisome isolation from senescent plants, carried out sample preparation for mass-spec analysis, and revised the manuscript. P.L. carried out the subcellular localization study of the HOL3 protein using onion cells and *Arabidopsis* protoplasts. S.T. participated in the cloning of YFP fusions of candidate genes. L.J.O. provided advice and support for peroxisome isolation. J.H. supervised the study and co-wrote the manuscript.

REFERENCES

Arai Y, Hayashi M, Nishimura M (2008) Proteomic analysis of highly purified peroxisomes from etiolated soybean cotyledons. **Plant Cell Physiol** 49: 526–539

Babujee L, Wurtz V, Ma C, Lueder F, Soni P, Van Dorsselaer A, Reumann S (2010) The proteome map of spinach leaf peroxisomes indicates partial compartmentalization of phylloquinone (vitamin K1) biosynthesis in plant peroxisomes. **J Exp Bot** 61: 1441–1453

Batzenschlager M, Masoud K, Janski N, Houlné G, Herzog E, Evrard J-L, Baumberger N, Erhardt M, Nominé Y, Kieffer B, Schmit A-C, Chabouté M-E (2013) The GIP gamma-tubulin complex-associated proteins are involved in nuclear architecture in *Arabidopsis thaliana*. **Front Plant Sci** 4: 480

Beevers H (1979) Microbodies in higher plants. **Annu Rev Plant Biol** 30: 159–193

Biswal UC, Biswal B (1984) Photocontrol of leaf senescence. **Photochem Photobiol** 39: 875–879

Buchanan-Wollaston V (1997) The molecular biology of leaf senescence. **J Exp Bot** 48: 181–199

Chen Z, Kastaniotis AJ, Miinalainen IJ, Rajaram V, Wierenga RK, Hiltunen JK (2009) 17-Hydroxysteroid dehydrogenase type 8 and carbonyl reductase type 4 assemble as a ketoacyl reductase of human mitochondrial FAS. **FASEB J** 23: 3682–3691

Corpas FJ, Barroso JB, Sandalio LM, Palma JM, Lupianez JA, del Río LA (1999) Peroxisomal NADP-dependent isocitrate dehydrogenase. Characterization and activity regulation during natural senescence. **Plant Physiol** 121: 921–928

Corpas FJ, Barroso JB, Carreras A, Quiros M, Leon AM, Romero-Puertas MC, Esteban FJ, Valderrama R, Palma JM, Sandalio LM, Gomez M, del Río LA (2004) Cellular and subcellular localization of endogenous nitric oxide in young and senescent pea plants. **Plant Physiol** 136: 2722–2733

Cutler SR, Ehrhardt DW, Griffitts JS, Somerville CR (2000) Random GFP::cDNA fusions enable visualization of subcellular structures in cells of *Arabidopsis* at a high frequency. **Proc Natl Acad Sci USA** 97: 3718–23

Desai M, Hu J (2008) Light induces peroxisome proliferation in *Arabidopsis* seedlings through the photoreceptor phytochrome A, the transcription factor HY5 HOMOLOG, and the peroxisomal protein PEROXIN11b. **Plant Physiol** 146: 1117–1127

Desai M, Pan R, Hu J (2017) *Arabidopsis* forkhead-associated domain protein 3 negatively regulates peroxisome division. **J Integr Plant Biol** 59: 454–458

Distefano S, Palma JM, McCarthy II, del Rio LA (1999) Proteolytic cleavage of plant proteins by peroxisomal

endoproteases from senescent pea leaves. **Planta** 209: 308–13

Dixon DP, Hawkins T, Hussey PJ, Edwards R (2009) Enzyme activities and subcellular localization of members of the *Arabidopsis* glutathione transferase superfamily. **J Exp Bot** 60: 1207–1218

Duncan O, Taylor NNLN, Carrie C, Eubel H, Kubiszewski-Jakubiak S, Zhang B, Narsai R, Millar AH, Whelan J (2011) Multiple lines of evidence localize signaling, morphology, and lipid biosynthesis machinery to the mitochondrial outer membrane of *Arabidopsis*. **Plant Physiol** 157: 1093–1113

Engqvist MKM, Schmitz J, Gertzmann A, Florian A, Jaspert N, Arif M, Balazadeh S, Mueller-Roeber B, Fernie AR, Maurino VG (2015) GLYCOLATE OXIDASE3, a Glycolate Oxidase Homolog of Yeast l-Lactate Cytochrome c Oxidoreductase, supports l-Lactate oxidation in roots of *Arabidopsis*. **Plant Physiol** 169: 1042–1061

Esser C, Kuhn A, Groth G, Lercher MJ, Maurino VG (2014) Plant and animal glycolate oxidases have a common eukaryotic ancestor and convergently duplicated to evolve long-chain 2-hydroxy acid oxidases. **Mol Biol Evol** 31: 1089–1101

Eubel H, Meyer EH, Taylor NL, Bussell JD, O'Toole N, Heazlewood JL, Castleden I, Small ID, Smith SM, Millar AH (2008) Novel proteins, putative membrane transporters, and an integrated metabolic network are revealed by quantitative proteomic analysis of *Arabidopsis* cell culture peroxisomes. **Plant Physiol** 148: 1809–1829

Fahy D, Sanad MNME, Duscha K, Lyons M, Liu F, Bozhkov P, Kunz H-H, Hu J, Neuhaus HE, Steel PG, Smertenko A (2017) Impact of salt stress, cell death, and autophagy on peroxisomes: Quantitative and morphological analyses using small fluorescent probe N-BODIPY. **Sci Rep** 7: 39069

Fukao Y, Hayashi M, Hara-Nishimura I, Nishimura M (2003) Novel glyoxysomal protein kinase, GPK1, identified by proteomic analysis of glyoxysomes in etiolated cotyledons of *Arabidopsis thaliana*. **Plant Cell Physiol** 44: 1002–1012

Fukao Y, Hayashi M, Nishimura M (2002) Proteomic analysis of leaf peroxisomal proteins in greening cotyledons of *Arabidopsis thaliana*. **Plant Cell Physiol** 43: 689–696

Gloerich J, Ruiter JPN, van den Brink DM, Ofman R, Ferdinandusse S, Wanders RJA (2006) Peroxisomal *trans* -2-enoyl-CoA reductase is involved in phytol degradation. **FEBS Lett** 580: 2092–2096

Gronemeyer T, Wiese S, Ofman R, Bunse C, Pawlas M, Hayen H, Eisenacher M, Stephan C, Meyer HE, Waterham HR, Erdmann R, Wanders RJ, Warscheid B (2013) The proteome of human liver peroxisomes: Identification of five new peroxisomal constituents by a label-free quantitative proteomics survey. **PLoS ONE** 8: e57395

Hooper CM, Castleden IR, Tanz SK, Aryamanesh N, Millar AH (2017) SUBA4: The interactive data analysis centre for *Arabidopsis* subcellular protein locations. **Nucleic Acids Res** 45: D1064–D1074

Hu J, Baker A, Bartel B, Linka N, Mullen RT, Reumann S, Zolman BK (2012) Plant peroxisomes: Biogenesis and function. **Plant Cell** 24: 2279–2303

Jiménez A, Hernández JA, Pastori G, del Río LA, Sevilla F (1998) Role of the ascorbate-glutathione cycle of mitochondria and peroxisomes in the senescence of pea leaves. **Plant Physiol** 118: 1327–1335

Kaur N, Hu J (2011) Defining the plant peroxisomal proteome: From *Arabidopsis* to rice. **Front Plant Sci** 2: 1–41

Kaur N, Hu J (2009) Dynamics of peroxisome abundance: A tale of division and proliferation. **Curr Opin Plant Biol** 12: 781–788

Kaur N, Reumann S, Hu J (2009) Peroxisome biogenesis and function. In: *The Arabidopsis Book* 7: p e0123

Koh S, André A, Edwards H, Ehrhardt D, Somerville S (2005) *Arabidopsis thaliana* subcellular responses to compatible *Erysiphe cichoracearum* infections. **Plant J** 44: 516–529

Li W, Zang B, Liu C, Lu L, Wei N, Cao K, Deng XW, Wang X (2011) TSA1 interacts with CSN1/CSN and may be functionally involved in *Arabidopsis* seedling development in darkness. **J Genet Genomics** 38: 539–546

Liebsch D, Keech O (2016) Dark-induced leaf senescence: New insights into a complex light-dependent regulatory pathway. **New Phytol** 212: 563–570

Lingner T, Kataya AR, Antonicelli GE, Benichou A, Nilssen K, Chen X-Y, Siemsen T, Morgenstern B, Meinicke P, Reumann S (2011) Identification of novel plant peroxisomal targeting signals by a combination of machine learning methods and *in vivo* subcellular targeting analyses. **Plant Cell** 23: 1556–1572

Lopez-Huertas E, Charlton WL, Johnson B, Graham IA, Baker A (2000) Stress induces peroxisome biogenesis genes. **EMBO J** 19: 6770–6777

Mi J, Kirchner E, Cristobal S (2007) Quantitative proteomic comparison of mouse peroxisomes from liver and kidney. **Proteomics** 7: 1916–1928

Nagatoshi Y, Nakamura T (2007) Characterization of three halide methyltransferases in *Arabidopsis thaliana*. **Plant Biotechnol** 24: 503–506

Nagatoshi Y, Nakamura T (2009) *Arabidopsis* HARMLESS TO OZONE LAYER protein methylates a glucosinolate breakdown product and functions in resistance to *Pseudomonas syringae* pv. *maculicola*. **J Biol Chem** 284: 19301–19309

Narendra S, Venkataramani S, Shen G, Wang J, Pasapula V, Lin Y, Kornyeyev D, Holaday AS, Zhang H (2006) The *Arabidopsis* ascorbate peroxidase 3 is a peroxisomal membrane-bound antioxidant enzyme and is dispensable for *Arabidopsis* growth and development. **J Exp Bot** 57: 3033–3042

Oh SA, Park JH, Lee GI, Paek KH, Park SK, Nam HG (1997) Identification of three genetic loci controlling leaf senescence in *Arabidopsis thaliana*. **Plant J** 12: 527–535

Ohno S, Nishikawa K, Honda Y, Nakajin S (2008) Expression in *E. coli* and tissue distribution of the human homologue of the mouse Ke 6 gene, 17β-hydroxysteroid dehydrogenase type 8. **Mol Cell Biochem** 309: 209–215

Palma JA, Jiménez A, Sandalio LM, Corpas FJ, Lundqvist M, Gómez M, Sevilla F, del Río LA (2006) Antioxidative enzymes from chloroplasts, mitochondria, and

peroxisomes during leaf senescence of nodulated pea plant. **J Exp Bot** 57: 1747–1758

Pan R, Hu J (2018) The Proteome of Plant Peroxisomes. In: del Río LA, Schrader M, eds. *Proteomics of Peroxisomes: Identifying Novel Functions and Regulatory Networks*. Springer, in press

Pan R, Kaur N, Hu J (2014) The *Arabidopsis* mitochondrial membrane-bound ubiquitin protease UBP27 contributes to mitochondrial morphogenesis. **Plant J** 78: 1047–1059

Pan R, Satkovich J, Hu J (2016) E3 ubiquitin ligase SP1 regulates peroxisome biogenesis in *Arabidopsis*. **Proc Natl Acad Sci USA** 113: 201613530

Panchuk II, Volkov RA, Schöffl F (2002) Heat stress- and heat shock transcription factor-dependent expression and activity of ascorbate peroxidase in *Arabidopsis*. **Plant Physiol** 129: 838–853

Paoletti AC, Parmely TJ, Tomomori-Sato C, Sato S, Zhu D, Conaway RC, Conaway JW, Florens L, Washburn MP (2006) Quantitative proteomic analysis of distinct mammalian mediator complexes using normalized spectral abundance factors. **Proc Natl Acad Sci USA** 103: 18928–18933

Pastori GM, del Rio LA (1997) Natural senescence of pea leaves (an activated oxygen-mediated function for peroxisomes). **Plant Physiol** 113: 411–418

Peterhansel C, Horst I, Niessen M, Blume C, Kebeish R, Kürkcüoglu S, Kreuzaler F (2010) Photorespiration. In: *The Arabidopsis Book 8*: p e0130

Quan S, Switzenberg R, Reumann S, Hu J (2010) *In vivo* subcellular targeting analysis validates a novel peroxisome targeting signal type 2 and the peroxisomal localization of two proteins with putative functions in defense in *Arabidopsis*. **Plant Signal Behav** 5: 151–153

Quan S, Yang P, Cassin-Ross G, Kaur N, Switzenberg R, Aung K, Li J, Hu J (2013) Proteome analysis of peroxisomes from etiolated arabidopsis seedlings identifies a peroxisomal protease involved in -oxidation and development. **Plant Physiol** 163: 1518–1538

Reumann S (2011) Toward a definition of the complete proteome of plant peroxisomes: Where experimental proteomics must be complemented by bioinformatics. **Proteomics** 11: 1764–1779

Reumann S, Babujee L, Ma C, Wienkoop S, Siemsen T, Antonicelli GE, Rasche N, Lüder F, Weckwerth W, Jahn O (2007) Proteome analysis of *Arabidopsis* leaf peroxisomes reveals novel targeting peptides, metabolic pathways, and defense mechanisms. **Plant Cell** 19: 3170–3193

Reumann S, Chowdhary G, Lingner T (2016) Characterization, prediction and evolution of plant peroxisomal targeting signals type 1 (PTS1s). **Biochim Biophys Acta - Mol Cell Res** 1863: 790–803

Reumann S, Ma C, Lemke S, Babujee L (2004) AraPerox. A database of putative *Arabidopsis* proteins from plant peroxisomes. **Plant Physiol** 136: 2587–2608

Reumann S, Quan S, Aung K, Yang P, Manandhar-Shrestha K, Holbrook D, Linka N, Switzenberg R, Wilkerson CG, Weber APM, Olsen LJ, Hu J (2009) In-depth proteome analysis of *Arabidopsis* leaf peroxisomes combined with in vivo subcellular targeting verification indicates novel metabolic and regulatory functions of peroxisomes. **Plant Physiol** 150: 125–143

Ribeiro CW, Korbes AP, Garighan JA, Jardim-Messeder D, Carvalho FEL, Sousa RHV, Caverzan A, Teixeira FK, Silveira JAG, Margis-Pinheiro M (2017) Rice peroxisomal ascorbate peroxidase knockdown affects ROS signaling and triggers early leaf senescence. **Plant Sci** 263: 55–65

Rodríguez-Serrano M, Romero-Puertas MC, Sanz-Fernández M, Hu J, Sandalio LM (2016) Peroxisomes extend peroxules in a fast response to stress via a reactive oxygen species-mediated induction of the peroxin PEX11a. **Plant Physiol** 171: 1665–1674

Sheehan D, Meade G, Foley VM, Dowd CA (2001) Structure, function and evolution of glutathione transferases: Implications for classification of non-mammalian members of an ancient enzyme superfamily. **Biochem J** 360: 1–16

Song Y, Yang C, Gao S, Zhang W, Li L, Kuai B (2014) Age-triggered and dark-induced leaf senescence require the bHLH transcription factors PIF3, 4, and 5. **Mol Plant** 7: 1776–1787

Sparkes IA, Baker A (2002) Peroxisome biogenesis and protein import in plants, animals and yeasts: Enigma and variations? (review). **Mol Membr Biol** 19: 171–185

Suzuki T, Nakajima S, Morikami A, Nakamura K (2005) An *Arabidopsis* protein with a novel calcium-binding repeat sequence interacts with TONSOKU/MGOUN3/BRUSHY1 involved in meristem maintenance. **Plant Cell Physiol** 46: 1452–1461

Tolbert NE, Oeser A, Yamazaki RK, Hageman RH, Kisaki T (1969) A survey of plants for leaf peroxisomes. **Plant Physiol** 44: 135–147

Vicentini F, Matile PM (1993) Gerontosomes, a multifunctional type of peroxisome in senescent leaves. **J Plant Physiol** 142: 50–56

Weaver LM, Amasino RM (2001) Senescence is induced in individually darkened *Arabidopsis* leaves, but inhibited in whole darkened plants. **Plant Physiol** 127: 876–886

Weaver LM, Gan S, Quirino B, Amasino RM (1998) A comparison of the expression patterns of several senescence-associated genes in response to stress and hormone treatment. **Plant Mol Biol** 37: 455–469

Wiederhold E, Veenhoff LM, Poolman B, Slotboom DJ (2010) Proteomics of *Saccharomyces cerevisiae* organelles. **Mol Cell Proteomics** 9: 431–445

Winter D, Vinegar B, Nahal H, Ammar R, Wilson GV, Provart NJ (2007) An "electronic fluorescent pictograph" Browser for exploring and analyzing large-scale biological data sets. **PLoS ONE** 2: e718

Yokouchl Y, Ikeda M, Inuzuka Y, Yukawa T (2002) Strong emission of methyl chloride from tropical plants. **Nature** 416: 163–165

SUPPORTING INFORMATION

Additional Supporting Information may be found online in the supporting information tab for this article: http://onlinelibrary.wiley.com/doi/10.1111/jipb.12670/suppinfo

Figure S1. Assessment of dark-induced senescence in *Arabidopsis*

Figure S2. Subcellular targeting analysis of GSA1 and FBA1.2

Figure S3. Subcellular targeting analysis of ACO3

Figure S4. Subcellular targeting analysis of RPL19A and GSTU20

Figure S5. Subcellular targeting analysis of RH37

Figure S6. Subcellular targeting analysis of GRP2 and GLX2-3

Figure S7. Subcellular targeting analysis of APX2

Figure S8. Subcellular targeting analysis of ATL65

Figure S9. Subcellular targeting analysis of AT3G47560 and PGL4

Figure S10. Subcellular targeting analysis of OARP1

Figure S11. Gene expression data from *Arabidopsis* eFP browser (bar.utoronto.ca)

Table S1. All protein identified in this study

Table S2. Non-peroxisomal proteins identified in this study

Table S3. Potentially new peroxisome proteins identified in this study

Table S4. Comparison of the proteome analyses of three major peroxisomal subtypes in *Arabidopsis*

Table S5. Primers and vectors used in this study

Scan using WeChat with your smartphone to view JIPB online

Scan with iPhone or iPad to view JIPB online